Growth is required for perception of water availability to pattern root branches in plants

Neil E. Robbins II[a,b] and José R. Dinneny[a,b,1]

[a]Department of Plant Biology, Carnegie Institution for Science, Stanford, CA 94305; and [b]Department of Biology, Stanford University, Stanford, CA 94305

Edited by Julian I. Schroeder, University of California, San Diego, La Jolla, CA, and approved December 12, 2017 (received for review June 13, 2017)

Water availability is a potent regulator of plant development and induces root branching through a process termed hydropatterning. Hydropatterning enables roots to position lateral branches toward regions of high water availability, such as wet soil or agar media, while preventing their emergence where water is less available, such as in air. The mechanism by which roots perceive the spatial distribution of water during hydropatterning is unknown. Using primary roots of *Zea mays* (maize) we reveal that developmental competence for hydropatterning is limited to the growth zone of the root tip. Past work has shown that growth generates gradients in water potential across an organ when asymmetries exist in the distribution of available water. Using mathematical modeling, we predict that substantial growth-sustained water potential gradients are also generated in the hydropatterning competent zone and that such biophysical cues inform the patterning of lateral roots. Using diverse chemical and environmental treatments we experimentally demonstrate that growth is necessary for normal hydropatterning of lateral roots. Transcriptomic characterization of the local response of tissues to a moist surface or air revealed extensive regulation of signaling and physiological pathways, some of which we show are growth-dependent. Our work supports a "sense-by-growth" mechanism governing hydropatterning, by which water availability cues are rendered interpretable through growth-sustained water movement.

hydropatterning | osmosensing | plant physiology | plant–water relations | root development

Water deficit strongly limits plant growth and development. While a number of strategies that plants use to cope with this stressor have been identified (1), details of the signaling pathways necessary for perception of water deficit are still poorly defined. In systems such as *Saccharomyces cerevisiae* traditional genetic approaches have been employed to elucidate water-perception pathways with considerable success (2). While similar approaches have succeeded in identifying candidate osmosensory proteins in plants (3–5), concerns regarding redundancy of signaling components and/or lethality associated with genetic knockouts suggest that alternative strategies may be necessary. In addition, many studies have focused primarily on understanding the function of signaling pathways that act at the single-cell level. Responses of plant roots to water availability, such as altered growth dynamics or tissue patterning, occur at the organ scale (1). These processes emerge from the actions of many cells and therefore may rely on the perception of environmental cues across the organ. Thus, an exploration of water perception using an organ-scale process as a model system may provide unique insight different from the scope of single-cell studies.

To explore how environmental cues pattern physiological responses at the organ scale we characterized water perception in the context of root hydropatterning, an organ-scale developmental response to variation in external water availability (1, 6). During hydropatterning lateral roots become activated in regions of the primary root directly contacting sources of available water, such as agar media, and fail to be induced where water is less available, such as air (Fig. 1 *A*–*C*). This phenomenon has been observed in several plant species and a wide variety of environmental contexts, including field soil (6).

To understand how water availability is perceived during hydropatterning we asked whether developmental competence for this environmental response is limited to specific regions along the length of the root. Developmental competence describes the ability of a cell or tissue to perceive and generate a response to a morphogenetic cue (7, 8). A number of mechanisms can give rise to competence, including the expression of proteins affecting signal perception, such as receptors and downstream signal-transduction components, or the absence of antagonists. We reasoned that determining the biological processes associated with developmental competence might provide clues on mechanisms of environmental perception and downstream signaling events.

In the following study we experimentally delineated the site of developmental competence for hydropatterning in *Zea mays* (maize) primary roots. This zone of competence closely correlated with the root growth zone, where cell expansion and water uptake occur. Mathematical modeling of water movement in this region suggested that a substantial growth-sustained difference in tissue water potential was present in the competent zone that distinguished tissues contacting external environments with high or low water availability. We show that tissue water potentials in the competent zone are strongly predictive of future patterns of lateral root emergence. These results implicate organ growth as an important contributing process in water perception in plant root tissues, representing a key advancement in our understanding of this phenomenon.

Significance

Plant roots activate lateral branching in response to contact with available water, but the mechanism by which this environmental signal is perceived is poorly understood. Through a combination of empirical and mathematical-modeling approaches we discovered a central role of tissue growth in this process. Growth causes water uptake, and the biophysical changes that occur during this process are interpreted by the organism to position new lateral branches. This observation is a significant advancement in our understanding of how the environment shapes plant development and demonstrates that perception of water is intimately tied to a core biological function of the root.

Author contributions: N.E.R. and J.R.D. designed research; N.E.R. performed research; N.E.R. contributed new reagents/analytic tools; N.E.R. and J.R.D. analyzed data; and N.E.R. and J.R.D. wrote the paper.

The authors declare no conflict of interest.

This article is a PNAS Direct Submission.

Data deposition: The data reported in this paper have been deposited in the Gene Expression Omnibus (GEO) database, https://www.ncbi.nlm.nih.gov/geo (accession no. GSE92406).

[1]To whom correspondence should be addressed. Email: dinneny@stanford.edu.

This article contains supporting information online at www.pnas.org/lookup/suppl/doi:10.1073/pnas.1710709115/-/DCSupplemental.

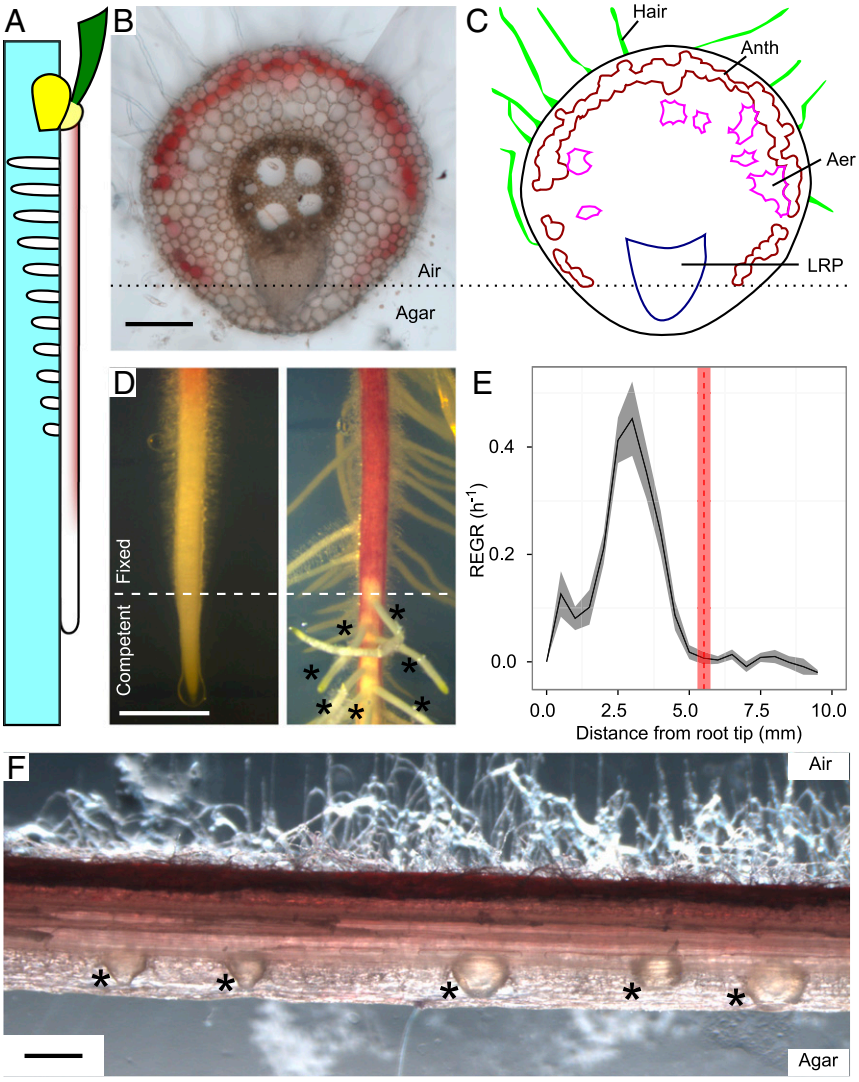

Fig. 1. Developmental competence to respond to water availability is limited to the root tip. (*A*) Diagram of maize seedling grown along agar media. Contact with agar (cyan box) locally activates lateral root development. (*B* and *C*) Unstained transverse section of primary root imaged by bright-field microscopy (*B*) and diagram highlighting environmentally regulated anatomical features (*C*). Dotted line, boundary between air and agar sides. Aer, aerenchyma; Anth, anthocyanin; Hair, root hair; LRP, lateral root primordium. (Scale bar, 250 μm.) (*D*) Air side of primary root immediately after application of agar sheet (*Left*) and following lateral root emergence 3 d later (*Right*). Asterisks indicate lateral roots that emerged toward the applied agar. Dashed line, boundary between competent and fixed zones. (Scale bar, 5 mm.) (*E*) Average relative elemental growth rate (REGR) (black, $n = 38$ seedlings) and position of competent/fixed-zone boundary (red, $n = 47$ seedlings). Shaded regions, SEM. Measurements are averages of three experimental replicates. (*F*) Unstained longitudinal section of primary root ∼4 cm from root tip imaged by bright-field microscopy. Section oriented with root tip pointing to left of image. Note the presence of lateral root primordia (*) exclusively on the agar side. (Scale bar, 500 μm.)

Results

The Competent Zone for Hydropatterning Coincides with the Growth Zone. Hydropatterning of lateral roots is readily studied in plant seedlings grown on the surface of an agar medium where one side of the root contacts the agar and the other side contacts the air in the headspace of the Petri dish. To determine which regions of root tissue are competent to respond to water availability during hydropatterning we applied an agar sheet to a previously air-exposed side of a primary root and tracked subsequent patterns of lateral root development (Fig. S1*A*). We predicted that developmentally competent regions would respond to agar application by producing new lateral roots, while regions which had lost competence would fail to do so. We used maize for this assay as it provided experimental advantages compared with *Arabidopsis*, a plant species used for much of the prior characterization of hydropatterning (6). Maize has a high density of lateral roots relative to the size of the different developmental zones of the primary root (Fig. S1) (∼7–10 lateral roots per cm primary root in maize vs. ∼1–3 in *Arabidopsis*). In addition, its larger diameter (1-mm diameter in maize vs. 0.1 mm in *Arabidopsis*) facilitates the use of micromanipulation and microdissection experimental approaches needed to precisely define the spatial domain of competence.

Following application of an agar sheet to the root we observed that lateral roots were induced within a defined region of the root. Developmental competence was clearly differentiated along the length of the root, with a distinct boundary separating responsive and unresponsive regions. We refer to tissues in the rootward direction of this boundary as the competent zone and those in the shootward direction as the fixed zone (Fig. 1*D*). Our results placed the competent-zone boundary within published ranges of the end of the root growth zone (9, 10). To evaluate this correlation further, we quantified local tissue expansion rates via kinematic growth analysis and found that under our experimental conditions the root growth zone was ∼5.34 ± 0.15 mm in length (11, 12). There was no significant difference between the measured longitudinal position on the root where hydropatterning competence was lost and where growth ceased (Fig. 1*E*, P = 0.9, mean difference ± SE = −0.03 ± 0.25 mm), indicating a strong correlation between these two developmental boundaries in the root tip. Past work in *Arabidopsis* showed that oscillating changes in auxin signaling necessary for lateral root patterning also occur at the end of the growth zone, consistent with this region being an important developmental zone across flowering plants (13). We did not observe obvious signs of arrested pre-emergence-stage lateral root primordia on the air side of maize primary roots, suggesting that hydropatterning of lateral root development occurs before lateral root initiation (Fig. 1*F*).

A Mathematical Model to Estimate Growth-Sustained Tissue Water Potentials. The strong correlation between growth and hydropatterning competence led us to ask whether growth itself was involved in the perception of water availability. In plant cells, growth is driven by cell wall loosening and concomitant water uptake (1, 14, 15). Although the air- and agar-contacting sides of a root have differential access to available water in our experimental system, there was no obvious sign of differential growth between these regions as roots generally grew straight along the agar surface. This indicated that rates of expansion, and therefore cellular water uptake, were equal between the two sides. Since most available water resides in the agar media, water must move across the root diameter to sustain cell expansion in air-exposed tissues. Water movement is driven by differences in water potential, or the chemical potential energy of water (1, 16, 17). Water moves from regions of high potential to low potential at a rate proportional to the difference in potential between the two regions. In order for water to move toward air-exposed tissues, we predicted that a substantial growth-sustained water potential gradient would occur in the root tip, which might also act as a biophysical cue to pattern lateral root development.

Growth-sustained water potential gradients have been proposed and empirically measured in the literature (18–21), but a role for them in tissue patterning has not yet been proposed or established. We asked to what extent a gradient existed in the competent zone, and whether it had any impact on lateral root patterning. To address this, we constructed a mathematical model to estimate water potentials of root tissues in our experimental conditions. We favored a computational approach over empirical measurement, as the former allows for more rapid investigation of a variety of environments. It also enables simulations to be performed, which can assist in identifying highly influential parameters that can be then be examined experimentally.

In the model the root was treated as a right circular cylinder divided into several segments along its longitudinal axis, with each segment subdivided into nine compartments (Fig. 2 *A* and *B*). The cylinder was assumed to be 1 mm in diameter, and tissue-layer dimensions were set based on dimensions measured from transverse sections of the primary root (e.g., Fig. 1*B*). Water was assumed to move freely between adjacent compartments in both the transverse and longitudinal directions and was allowed to enter or exit root tissues via external water sources (agar media or air) at various points along the perimeter of the tissue. Water potentials of external agar media were assumed to be −0.1 MPa, unless empirically measured. Because our tissue culture plates were completely sealed with Parafilm, the water potential of air was assumed to be in equilibrium with the surrounding agar media. The model can simulate water delivery via the phloem (22, 23), but because there are no empirical data on the relative contributions of internal and external water sources for maize primary root growth at the seedling stage we assumed all water uptake was externally derived, unless otherwise noted.

The network of root compartments was modeled as a hydraulic circuit, with each compartment represented as a node in the circuit (Fig. 2 *C* and *D*). The rate of water uptake for each compartment was estimated based on empirical growth-rate measurements. Since we assumed all growth occurred in the longitudinal dimension, growth could be modeled as a change in compartment height, and therefore volume, over time (Fig. 2*E*). Ninety percent of this volume change was assumed to be attributable to water uptake, based on water content values cited for similar tissues (16). The resistance of water movement between each node is measured by the reciprocal of hydraulic conductivity (1, 16). We used a literature-derived value of 1.15×10^{-7} $m^{-3} \cdot m^{-2} \cdot s^{-1} \cdot MPa^{-1}$ for maize root tissue conductivity (24). Although we considered this previously published study to be the best approximation for our purposes based on the tissue region of interest and method of measurement, we acknowledge that conductivity can vary considerably from study to study (25–27). For this reason, we compared model outputs across a range of conductivity values at a later point in our analysis.

Differences in compartment water potentials, analogous to differences in voltage, were calculated using the following equation: $J_V = \Delta\Psi_w \times Lp \times A$. In this equation J_V is the rate of water flow between two compartments (cubic meters per second), $\Delta\Psi_w$ is the water potential difference (megapascals), Lp is hydraulic conductivity (cubic meters per square meter per second per megapascal), and A is the surface area of the interface between the compartments (square meters). Since water potential is the only unknown value in the above relationship, it can be calculated algebraically using a system of linear equations derived using Kirchhoff's circuit laws (28) (Fig. 2*F*). We wrote an algorithm in the R programming language to generate and solve this system of equations, which is freely available for download in a Github repository (https://github.com/nerobbin/20161214_hydropatterning).

As a proof-of-concept test for the ability of this method to accurately estimate tissue water potential we applied it to *Glycine max* hypocotyls, the only growing plant organ for which empirical measurements of cellular water potential at the tissue scale are available (19) (Fig. S2). We updated the model to take into account tissue organization and hydraulic parameters unique to this organ. The accuracy of our model predictions depended largely on the value used for tissue hydraulic conductivity, with highest accuracy obtained at a value within the range of those previously reported (29). Discrepancies between overall profiles of empirical and estimated water potentials hinted at tissue-specific variation in conductivity not taken into account by the model, which assumes uniform conductivity. The absence of higher-resolution measurements of tissue hydraulic conductivity, and the experimental challenges associated with making such measurements, make bulk-tissue values a necessary approximation in our model.

We then applied the model to simulate maize roots growing along an agar medium. Local tissue water potentials were predicted to decrease as local growth rate increased, with the largest decreases that we predicted being in tissues most distal to the external water source, thus generating a differential across the diameter of the root (Fig. 2*G*). Notably, we found that all tissues approached water potential equilibrium after growth ceased, demonstrating the necessity of growth for sustaining potential gradients. These results suggest that substantial differentials in water potential exist between air- and agar-contacting tissues in the competent zone (peak differential in the epidermis = −0.75 MPa, cortex = −0.34 MPa).

Modeling Relates Growth and Water Uptake to Lateral Root Patterning. To determine whether tissue water potentials play a role in hydropatterning we first tested whether there was a quantitative relationship between tissue water potential and lateral root development. Tissue growth rates and lateral root distributions were measured in seedlings grown between two agar sheets containing differing concentrations of PEG, which was used to alter external water availability over a wide range of values (Fig. 3 *A*–*C*).

Measured growth rates and external water availabilities were then used in our model to estimate tissue water potentials. We focused our attention on water potentials of the epidermal layer, as prior research implicated outer tissue layers as important sites of early hormonal signaling events upstream of water-induced lateral root initiation (6). We further restricted our analysis to potentials occurring within the competent zone. While our previous experiment delineated the shootward boundary of the competent zone, the rootward boundary required further experimentation to determine. The location of this boundary was

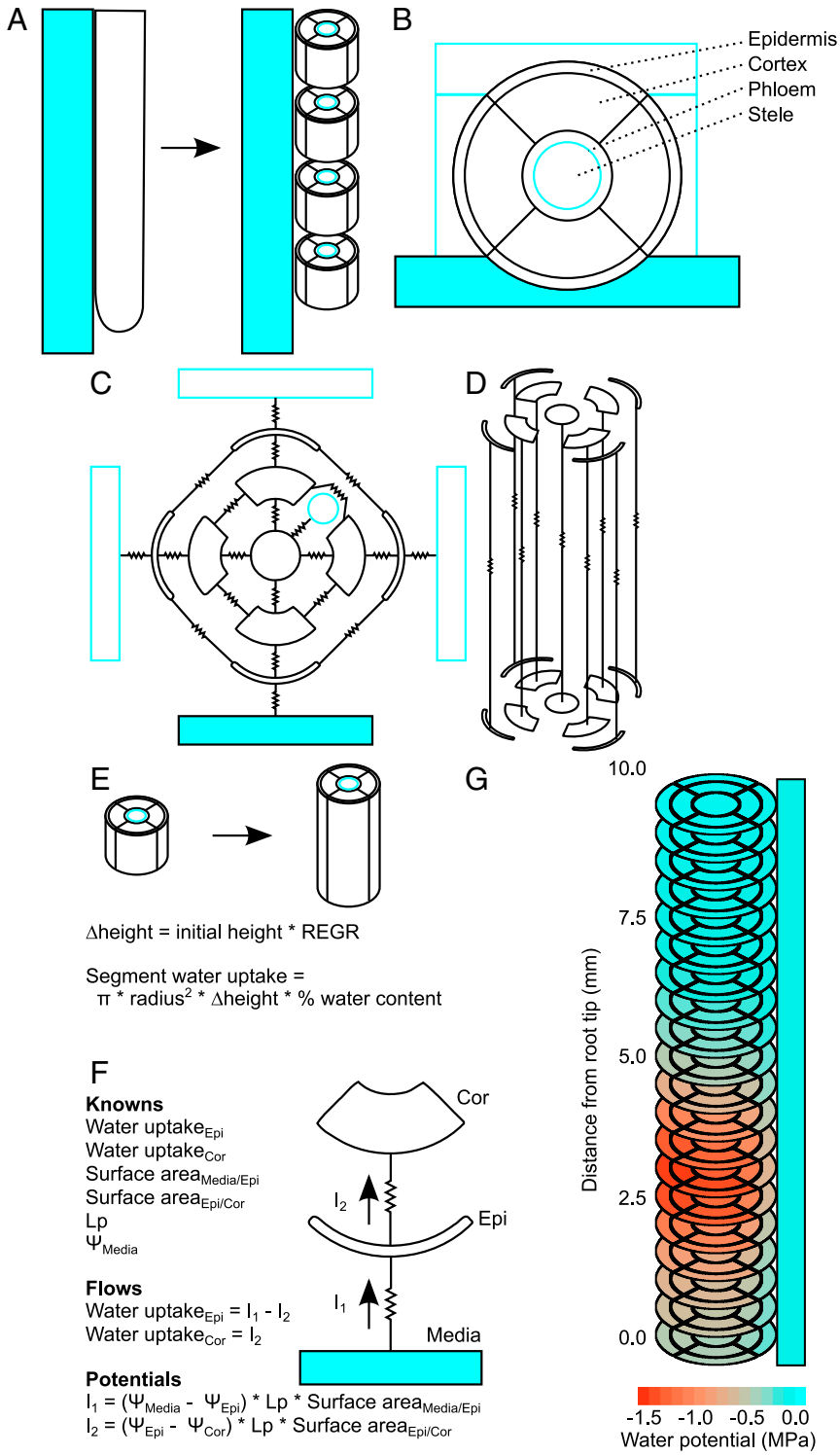

Fig. 2. Mathematical modeling of tissue water potentials in the growth zone. (*A*) A root growing along agar (filled cyan box) is treated as a series of right circular cylinders. (*B*) Each segment is divided into compartments. Water can be taken up externally via agar or air (hollow cyan box) or internally via the phloem (cyan ring). (*C* and *D*) The network of root compartments is modeled as a hydraulic circuit. Connections for radial (*C*) and longitudinal (*D*) water flow are shown. (*E*) Growth is modeled as a change in cylinder height over time, calculated based on relative elemental growth rate (REGR). A user-specified value (percentage water content) dictates the amount of volume change attributable to water uptake. (*F*) Example calculation of compartment water potentials (Ψ). Compartment water uptake and surface areas are calculated based on total water uptake and compartment geometry. Hydraulic conductivity (Lp) and media water potential (Ψ_{Media}) are user-specified. Intercompartment water flow rates (I, arrows) are determined using a system of equations ("Flows"), and are then used to calculate compartment water potentials in a second system of equations ("Potentials"). (*G*) Estimated tissue water potentials based on REGR curve in Fig. 1*E*.

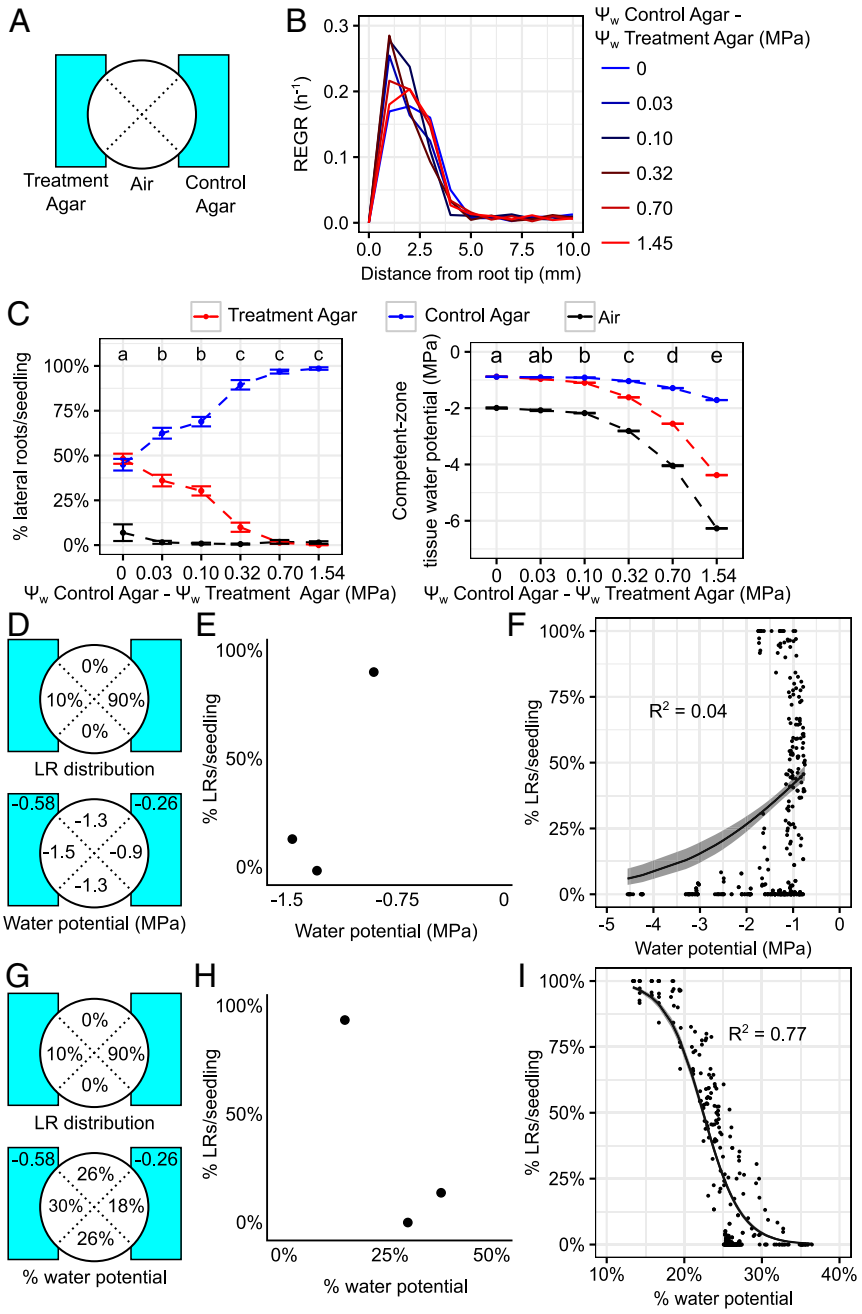

Fig. 3. Tissue water potential is predictive of lateral root patterning. (*A*) Diagram of experimental setup. Primary roots were grown between two agar sheets, with varying concentrations of PEG applied in the treatment agar. Dotted lines denote division of primary root for lateral root quantification. (*B* and *C*) Relative elemental growth rate (REGR) profiles (*B*), lateral root (LR) distributions (*C*, *Left*), and model-estimated competent-zone tissue water potentials (*C*, *Right*) under indicated treatment conditions. Air-side data are sums of the two air-exposed quadrants depicted in *A*. Samples grouped based on average water potential (Ψ_w) difference between the two agar sheets. Error bars denote SE. SEs in *B* were omitted for legibility and averaged at ± 0.02 h^{-1} in the region 0–6 mm from the root tip. Significantly different groups are denoted with different letters ($P < 0.05$). n = 14–16 seedlings per condition across two experiments. (*D* and *E*) Illustration of method used to plot tissue water potentials and lateral root distributions for regression analysis. Values in each root quadrant for a single seedling are shown (*D*). Media water potentials (megapascals) are shown as numbers within cyan boxes. Data from each quadrant are then plotted in a scatter plot as a single point (*E*). (*F*) Scatter plot of data from individual seedlings averaged in *C* plotted using strategy shown in *E*. Curve and shaded region, mean ± SE of best-fit line for zero–one inflated beta regression model. R^2, pseudo-R^2 value. (*G* and *H*) Repeat of previous example (*D* and *E*) using normalized (percent) water potential values. Normalization was done by dividing each quadrant value by the sum of all quadrants. (*I*) Unaveraged data from *C* plotted as shown in *H*.

determined by applying small agar sheets to the air-exposed side of the primary root. We reasoned that an agar sheet as large as or larger than the competent zone would be inductive for lateral root development, while a sheet smaller than the competent zone would fail to do so. The minimal inductive sheet size therefore provides an approximation for the size of the competent zone and can be used to calculate the position where the zone begins. The smallest sheet capable of inducing lateral root production was 1.54 mm (Fig. S3), suggesting that the competent zone lay between ∼4.0 and 5.5 mm from the root tip at the distal end of the growth zone.

Competent-zone water potentials were summed for each epidermal quadrant and plotted against relative lateral root distributions (Fig. 3 *D*–*F*). We focused on relative distributions of lateral roots in our analysis to avoid any effects of changes in overall lateral root density that might occur independent of changes in distribution (Fig. S4). While absolute water potential did not show a strong relationship with lateral root patterning, we speculated that normalizing the water potential values might reveal a clearer relationship. We tested two normalization methods: one that converted water potentials to percentages (Fig. 3 *G* and *H*) and another that involved mean-centering the water potential values. Interestingly, both normalization schemes revealed clear sigmoidal relationships in the data (Fig. 3*I* and Fig. S5). Such normalization is physiologically relevant, since water movement depends entirely on relative differences in water potential rather than absolute values. While our analysis is unable to distinguish which normalization is more biologically meaningful, goodness-of-fit statistics best supported the percentage normalization method. A zero–one inflated beta regression model using these values explained 77% of the variance

in the dataset, indicating high predictive power of local water potentials for lateral root patterning.

Our regression model exhibited systematic biases within certain ranges of tissue water potential, suggesting inaccuracies in our water potential estimates for some data points. To test whether this was caused by misparameterization of tissue hydraulic conductivity we refit the model using a range of different values. We observed substantial improvement in model fit (R^2 = 0.85–0.91) at conductivities at or below ~5×10^{-8} $m^3 \cdot m^{-2} \cdot s^{-1} \cdot MPa^{-1}$ (Fig. S6). This observation suggests that tissue conductivity may be lower than our assumed reference value (1.15×10^{-7} $m^3 \cdot m^{-2} \cdot s^{-1} \cdot MPa^{-1}$), perhaps due to suborgan variation in conductivity and/or changes resulting from the treatment conditions examined. We noted that model fit plateaued within the above range of conductivity values, suggesting that the fit was unlikely to improve as conductivity was further decreased beyond physiologically relevant values. Although a deeper understanding of root tissue conductivity in our experimental setup would likely improve model fit, our current model nonetheless explains a substantial portion of the variation in lateral root distribution. We therefore continued our analysis with the empirically determined conductivity value.

Our regression model allowed us to make predictions regarding how biophysical properties of the root and its environment might impact hydropatterning. The model predicted that primary roots with smaller diameters would have a higher frequency of air-side lateral roots, which may explain previous observations of weaker hydropatterning in *Arabidopsis* compared with species like maize or *Oryza sativa* (rice) (Fig. S7*A*) (6). Increasing the contribution of phloem-derived water to overall root water uptake had no substantial effect on model predictions (Fig. S7*B*). Variation in tissue hydraulic conductivity had a large effect on predicted lateral root distribution, but only for conductivity in the transverse direction (Fig. S7*C*). Altering conductivity for longitudinal water flow had a weak effect on model predictions, and there did not appear to be synergistic effects between the two conductivity values (Fig. S7 *D* and *E*).

This analysis was by no means an exhaustive assessment of all combinations of parameter values. Thus, we have generated an R Shiny app that allows readers to explore the full parameter space using an interactive graphical user interface (https://nrobbins.shinyapps.io/20171008_hydropatterning_app/). Raw data used for fitting and validation of the regression model can also be found in a Github repository (https://github.com/nerobbin/20161214_hydropatterning).

Growth Dynamics Affect Hydropatterning of Lateral Root Development. Given the strong correlation between growth and competence for hydropatterning, we examined the predicted effects of altering growth dynamics on branching pattern using our model (Fig. 4 *A* and *B*). Interestingly, the frequency of lateral root initiation toward air increased as the end of the growth zone was shifted rootward and away from the competent/fixed-zone boundary. This was more pronounced at lower values of peak elemental growth rate, suggesting a synergistic interaction between the two factors. We note that these simulations were performed assuming constant position and size of the competent zone, which caused uncoupling of growth from competence. Contrastingly, the effect of growth zone position on lateral root patterning was strongly reduced when the competent zone was configured to track with the growth zone (Fig. 4*C*). This indicated that tight coordination between growth as a signal generator and competence as a signal receiver were likely to be important for hydropatterning.

Based on these simulations we hypothesized that the ability of the root to locally distinguish regions of high and low water availability may depend on the overall rate of growth-sustained water uptake in the competent zone. To test this hypothesis we scored lateral root patterning in seedlings exposed to different growth inhibitors. Seedlings were treated with sodium

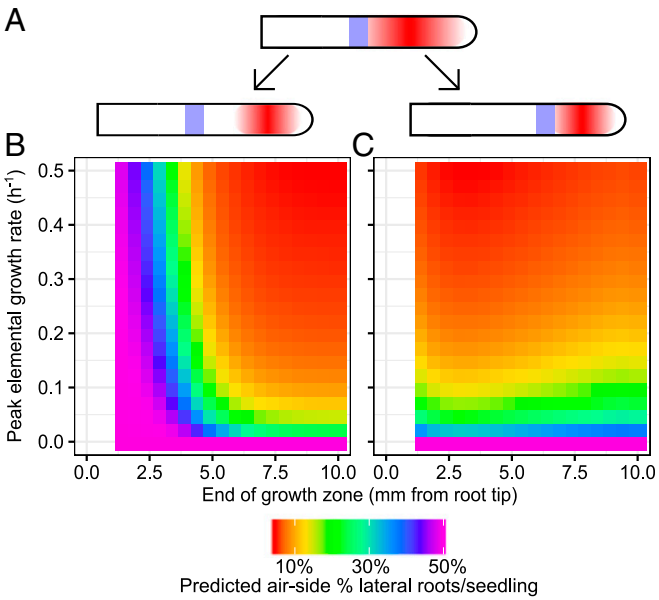

Fig. 4. Modeling predicts a disruption of hydropatterning when growth is perturbed. (*A*) Schematic of simulated changes in growth- and competent-zone positions. (*Top*) A root with standard growth-zone (red) and competent-zone (blue) positions. (*Bottom Left*) Growth zone position varied while competent zone remained constant. (*Bottom Right*) Competent zone position tracked with the growth zone. (*B* and *C*) Predicted frequency of air-side lateral root initiation with varied growth-zone parameter values. Competent zone was set to remain stationary (*B*), or track with the position of the growth zone (*C*). Start of growth zone was set to 0 mm from the root tip in all simulations. Predictions were generated for primary roots grown between two agar sheets.

orthovanadate (Na_3VO_4) and diethylstilbestrol (DES), two inhibitors of plasma membrane H^+-ATPases which partly function to acidify the cell wall and promote wall-loosening expansin activity during cell elongation (14, 30–32). Interestingly, hydropatterning was disrupted in treatment conditions that also reduced growth (Fig. 5 *A* and *B* and Dataset S1). Comparable results were obtained using citric acid, which increases pH-buffering capacity of the external medium, as well as low-temperature stress (Fig. 5 *A* and *B* and Dataset S1). Empirical observations of lateral root patterning in these different conditions significantly correlated with predictions of our regression model, with correlation coefficients between 0.65 and 0.97 depending on treatment condition ($P < 0.0002$; Fig. 5*C*). This variation in correlation is suggestive of treatment-specific effects on lateral root patterning that are independent of alterations to growth dynamics. Nonetheless, these observations provide validation of the predictive power of the model under a broad range of conditions and support our hypothesis that growth is required for lateral root hydropatterning.

We then sought to identify signaling processes involved in hydropatterning downstream of growth. We quantified hydropatterning in a panel of genetically diverse inbred lines from the maize nested association mapping (NAM) population (33). Several lines from this population exhibited poor germination or failed to produce lateral roots in our conditions and thus could not be phenotyped. We identified one inbred, Oh7B, that showed a significantly higher frequency of air-side lateral root emergence compared with our reference inbred, B73 (Fig. 5*D*). Interestingly, growth dynamics in Oh7B did not significantly differ from B73, indicating that growth alone could not explain the observed difference in hydropatterning (Fig. 5*E*). This suggests that growth is partially uncoupled from lateral root patterning in Oh7B, perhaps by genetic variation in downstream signaling components necessary for linking these two processes.

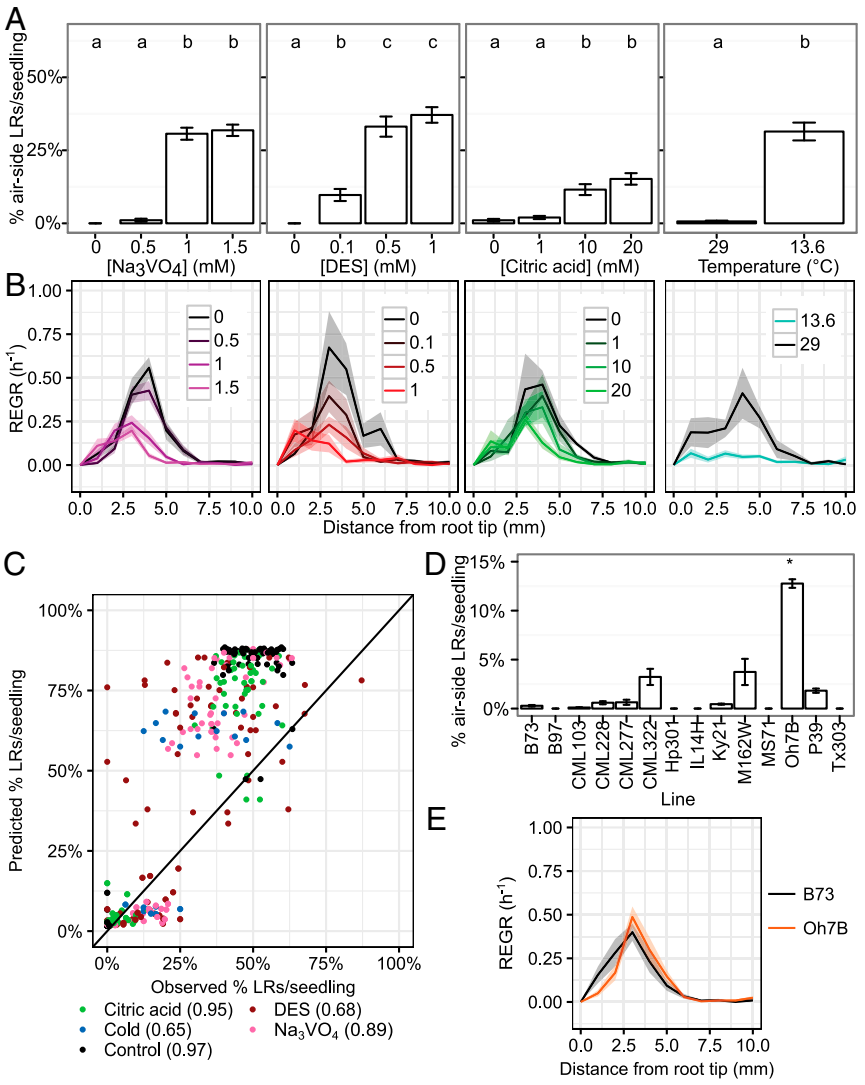

Fig. 5. Growth is necessary for lateral root hydropatterning. (*A* and *B*) Air-side lateral root (LR) emergence frequency (*A*) and relative elemental growth rate (REGR) (*B*) in indicated condition. Primary roots were grown between two agar sheets, with lateral roots quantified in the air gap between the sheets. Chemical treatments were added to both agar sheets. Significantly different groups are denoted with different letters ($P < 0.05$). (*C*) Observed and model-predicted lateral root distributions for samples in *B*. Diagonal line denotes perfect prediction by the model. Values in parentheses denote Pearson's correlation coefficient for comparison of empirical and predicted values. Each coefficient significantly differed from 0 ($P < 0.0002$). (*D*) Air-side lateral root emergence frequency in indicated inbred line. Seedlings were grown along one agar surface. Asterisk indicates significant difference from B73 ($P < 0.05$). (*E*) REGR for B73 and Oh7B seedlings grown between two agar surfaces. $n = 10$–16 (*A*), 7–8 (*B* and *C*), 5–15 (*D*), and 8 (*E*) seedlings per treatment level or genotype across two experiments. Additional replicates of lateral root phenotyping under Na_3VO_4 treatment and for Oh7B can be found in Fig. S8.

Comparative genomic studies of B73 and Oh7B may therefore uncover molecular actors involved in water transport, perception, or signaling.

Growth Perturbation Results in Altered Patterns of Gene Expression. To determine the broader downstream impact that growth-sustained water potentials have on cellular signaling and physiology we performed transcriptomic profiling of longitudinal domains of the root corresponding to the competent and fixed regions and separately profiled tissue in contact with air or agar (Fig. 6*A* and Dataset S2; and Gene Expression Omnibus database accession no. GSE92406). We detected a total of 25,835 unique transcripts, 1,559 of which were significantly differentially expressed between the air- and agar-exposed sides of the root. Of these, 1,461 were differentially expressed in the fixed zone, suggesting that the functional divergence of the two sides occurred primarily after competence was lost.

The side-biased transcriptome included a number of pathways known to be affected by hydropatterning, including anthocyanin biosynthesis, root hair development, programmed cell death, lignin accumulation, and signaling associated with the plant hormone auxin (6, 34). Several genes up-regulated on the agar side encoded LATERAL ORGAN BOUNDARIES (LOB) domain transcription factors, including ROOTLESS CONCERNING CROWN AND SEMINAL LATERAL ROOTS (RTCS) (35). *RTCS* homologs in *Arabidopsis* and rice are involved in early stages of lateral root development (36–39), suggesting that these genes may serve as markers of this process in maize. Our analysis revealed other pathways regulated during hydropatterning, including brassinosteroid and ethylene signaling, and water transport. The majority of these side-biased pathways appear in the fixed zone and provide insights on downstream consequences of water perception.

We also compared the transcriptomes of competent and fixed tissues on the two sides of the root to determine how gene expression changed during this developmental transition (Dataset S3); 12,055 genes were significantly differentially expressed between the two zones independent of the side of the root queried, suggestive of a large cohort of developmentally regulated genes that are unresponsive to environmental inputs. Gene Ontology (GO) analysis identified enrichment of genes likely involved in meristem function in the competent zone (translation, chromatin organization, DNA replication, and cell cycle control) and genes related to Casparian strip formation and other aspects of developmental maturation in the fixed zone (abiotic and biotic stress response, hormone response, and phenylpropanoid metabolism) (Dataset S4).

A smaller set of genes was found to vary between the two zones in a side-dependent manner (Dataset S3). GO analysis was largely unable to identify enrichment of functional categories

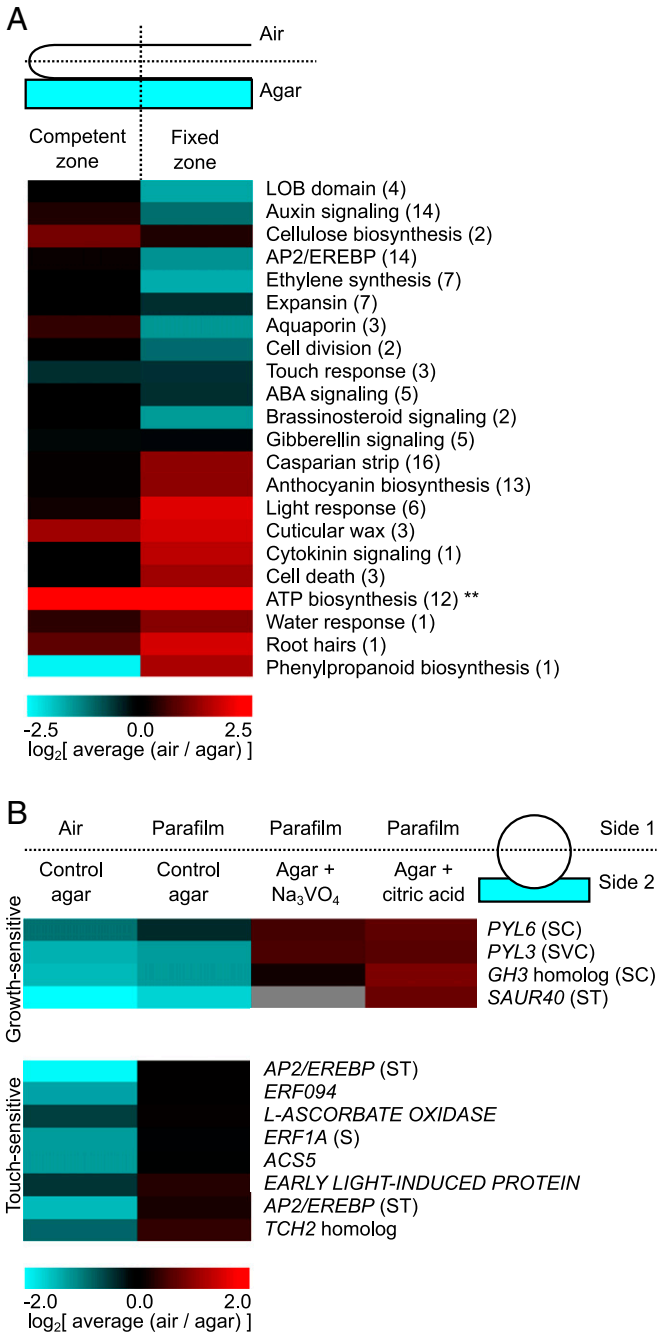

Fig. 6. Growth plays a role in regulation of gene expression by water availability. (*A*) Expression patterns of side-biased gene categories identified by RNA sequencing (RNA-Seq). Seedlings were grown along a single agar surface and sectioned according to diagram (*Top*). Air/agar FPKM (fragments per kilobase million) ratio was computed for each gene and averaged by category. Resulting values were then log-transformed. Number of genes per category are indicated in parentheses. **Values for ATP biosynthesis were outliers (6.34 and 6.77 for competent and fixed zones, respectively) and are plotted as 2.5. (*B*) Expression patterns of a subset of genes identified in *A* measured by RT-qPCR. Seedlings were grown between agar and indicated low-water availability substrate (*Top*). Agar was supplemented with 1.5 mM Na_3VO_4 or 20 mM citric acid where indicated. Air/agar relative expression ratio (arbitrary units) was computed for each gene and log-transformed. Parentheses denote genes identified as statistically significantly regulated ($P < 0.05$): C, citric acid-sensitive; S, side-biased in air/control agar and Parafilm/control agar; T, touch-sensitive; V, Na_3VO_4-sensitive. Growth-sensitive and touch-sensitive gene clusters identified based on hierarchical clustering. Data are shown for fixed-zone tissues. $n = 3$ pools of two seedlings each for each tissue section for both *A* and *B*. Gray box denotes insufficient data to perform calculations.

among these genes, with RNA processing specific to the competent zone on the air side being the only major function identified (Dataset S4). Examination of the most highly differentially expressed genes in this set revealed several encoding kinases and calcium-signaling proteins specific to the fixed zone on the contact side, suggestive of changes in signaling unique to water-contacting tissues. While these data provide an examination of the transcriptional changes that occur in response to local contact of tissues with water or air, further analysis is required to determine which, if any, of these transcriptionally regulated genes may be components of the signaling pathway necessary for perception of water availability.

To test the role that growth has in determining these gene expression patterns we used high-throughput RT-qPCR to quantify expression of a panel of side-biased genes in seedlings treated with Na_3VO_4 or citric acid (Fig. 6*B* and Dataset S6). To determine if differentially expressed genes were responsive to water availability or mechanical contact we compared roots exposed to air and agar with roots grown between agar and a sheet of Parafilm to simulate contact with a non-water-conducting surface. A subset of the genes examined were equally induced by Parafilm and control media, indicating that mechanical contact alone was likely responsible for their induction by agar (touch-induced). Among the genes that were induced by agar and not touch alone we identified several that lost their water-biased expression under growth inhibition. Within this set were genes in the auxin pathway, as well as members of the *PYRABACTIN RESISTANCE1/PYR1-LIKE* (*PYL*)/*REGULATORY COMPONENT OF ABA RECEPTORS* family of receptors for abscisic acid, a hormone broadly involved in responses to water-deficit stress (40). The expression pattern of all water-responsive genes tested was affected by growth inhibition. However, this does not preclude the presence of growth-independent pathways for water perception operating within the root. A more thorough examination of the water-responsive transcriptome may reveal evidence in support of this possibility. Nonetheless, the above observations demonstrate that a portion of the water-responsive transcriptome is sensitive to changes in growth dynamics, providing evidence of a more general role for growth in the response of the root to water availability.

Discussion

Together, our data support a model in which growth-dependent water uptake, in conjunction with spatial heterogeneity in local water availability, generates internal gradients of tissue water potential that inform developmental patterning and gene expression (Fig. 7). Thus, growth induces a physical state in which water perception can occur. This "sense-by-growth" mechanism illustrates that the perception of water is dependent on a state of disequilibrium established by the organism that allows meaningful spatial information to be derived from the external environment. Our work represents a significant advance in our understanding of the processes governing water sensing in plants, as it connects perception of a key environmental resource to a central physiological function of the organ.

This conclusion is based partly on results from mathematical modeling, which showed that estimates of tissue water potential are strongly predictive of lateral root patterning. The precise nature of this relationship depends largely on assumed parameter values, with tissue hydraulic conductivity being the most influential of those examined. Improving the model would require more refined measurements of conductivity that take into account variation between tissue layers and paths of water movement (41). Advances in water tracking using Raman spectroscopy, which can distinguish between water molecules containing different hydrogen isotopes with high spatial and temporal resolution, make this a promising tool for such experiments (42–44).

While these efforts would improve the model, direct measurement of tissue water potential will best circumvent the issues

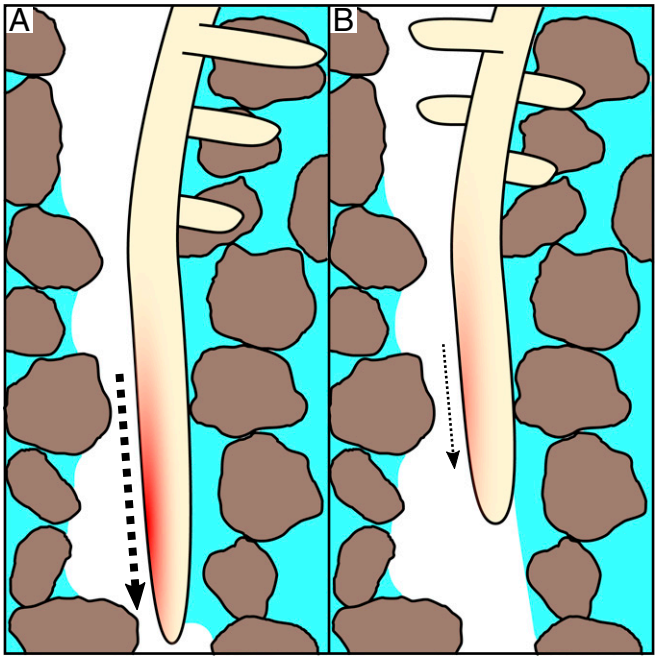

Fig. 7. A sense-by-growth mechanism for water perception. (*A*) A primary root grows along an air–water interface (white and cyan, respectively) in a network of soil particles (brown). Rapid growth (dashed arrow) leads to induction of a strong internal water potential gradient (red) that drives patterning of lateral-root branches toward areas of high water availability. (*B*) A root with slower growth (dashed arrow) induces a weaker water potential gradient and positions lateral roots in areas of both high and low water availability.

associated with inaccurate parameterization. However, current technology for accomplishing this, the pressure probe (45), is highly invasive and would likely be difficult to adapt to the seedling growth conditions used in this study. Optical sensors of cellular water potential, akin to a macromolecular crowding sensor developed previously (46), would be a useful alternative. These would be more versatile and less invasive than the current approach, and could also open new avenues of research on plant–water relations at the microscale.

The physiological mechanism for water perception proposed here provides clues toward identifying molecular–genetic actors in this pathway. Key to this pursuit is our identification of the competent zone for water responsiveness, located at the end of the root growth zone. We hypothesize that the molecular machinery for water perception is likely to be expressed and active within this region of tissue. Although our transcriptional analysis did not identify clear candidates for genes that play this role, it is possible that time-course analysis of molecular events immediately following water application may be more informative. Our discovery of altered hydropatterning in the maize inbred Oh7B provides another potential avenue for genetic studies. Since this inbred is included in the NAM population, mapping of genetic loci associated with this phenotype using quantitative trait locus analysis will likely be relatively straightforward.

In addition, our results provide a framework for understanding the role of hydropatterning under water deficit in the field. Current understanding of root-system architecture posits the existence of root ideotypes, idealized architectures suited to specific environmental contexts (47). We speculate that strong hydropatterning would be most suitable in environments that experience prolonged water deficit, as stricter placement of lateral roots would limit resource expenditure toward exploring water-poor regions of soil. Contrastingly, weak hydropatterning may be useful in fluctuating water conditions, where short-term costs associated with branching in low-water areas would be offset by an enhanced ability to capture later influxes of water. Alternatively, weak hydropatterning may allow for the uptake of resources, such as phosphorus, present in the upper layers of soil, which generally dry faster. The weak-hydropatterning phenotype of Oh7B can be leveraged to test these hypotheses in field trials. Once the effects of altered hydropatterning are clarified, targeted modification of root biophysical parameters (e.g., tissue conductivity) could be performed to tune lateral root patterning to fit a variety of watering regimes. Our mathematical model could help guide these efforts by enabling specific modifications to be tested in silico before being carried out *in planta*.

These and other future studies proposed here will be key to advancing our overall understanding of plant water perception and its impact on root-system architecture. Knowledge of this will be integral to improving crop water-use efficiency to meet the demands of a growing world population.

Materials and Methods

Plant materials and methods for plant growth, kinematic growth analysis, competent zone determination, mathematical modeling, lateral root quantification, and transcriptional analyses can be found in *SI Materials and Methods*.

ACKNOWLEDGMENTS. We thank Robert E. Sharp, John S. Boyer, Kenneth A. Shackel, and Wendy K. Silk for inspiration and suggestions on experimental design; Silk and members of the J.R.D. laboratory for critical evaluation of the content of the manuscript; and Wei Feng for performing independent replication of key experiments (Fig. S8). This work was supported by the Carnegie Institution for Science Endowment and the National Science Foundation's Plant Genome Research Program (Grant IOS-PGRP 420-40-45A) (to J.R.D.). Research reported in this publication was supported by the National Institute of General Medical Sciences of the National Institutes of Health under Award T32GM007276. The content is solely the responsibility of the authors and does not necessarily represent the official views of the National Institutes of Health. This material is based upon work supported by the National Science Foundation Graduate Research Fellowship under Grant DGE-1147470. Any opinion, findings, and conclusions or recommendations expressed in this material are those of the author(s) and do not necessarily reflect the views of the National Science Foundation.

1. Robbins NE, 2nd, Dinneny JR (2015) The divining root: Moisture-driven responses of roots at the micro- and macro-scale. *J Exp Bot* 66:2145–2154.
2. O'Rourke SM, Herskowitz I, O'Shea EK (2002) Yeast go the whole HOG for the hyperosmotic response. *Trends Genet* 18:405–412.
3. Yuan F, et al. (2014) OSCA1 mediates osmotic-stress-evoked Ca2+ increases vital for osmosensing in Arabidopsis. *Nature* 514:367–371.
4. Wilson ME, Basu MR, Bhaskara GB, Verslues PE, Haswell ES (2014) Plastid osmotic stress activates cellular stress responses in Arabidopsis. *Plant Physiol* 165: 119–128.
5. Hamilton ES, et al. (2015) Mechanosensitive channel MSL8 regulates osmotic forces during pollen hydration and germination. *Science* 350:438–441.
6. Bao Y, et al. (2014) Plant roots use a patterning mechanism to position lateral root branches toward available water. *Proc Natl Acad Sci USA* 111:9319–9324.
7. Scott MP (2000) Development: The natural history of genes. *Cell* 100:27–40.
8. Waddington CH (1932) III. Experiments on the development of chick and duck embryos, cultivated *in vitro*. *Philos Trans R Soc Lond B Biol Sci* 221:179–230.
9. Ishikawa H, Evans ML (1995) Specialized zones of development in roots. *Plant Physiol* 109:725–727.
10. Sharp RE, Silk WK, Hsiao TC (1988) Growth of the maize primary root at low water potentials: I. Spatial distribution of expansive growth. *Plant Physiol* 87:50–57.
11. Erickson RO (1976) Modeling of plant growth. *Annu Rev Plant Physiol* 27:407–434.
12. Erickson RO, Silk WK (1980) The kinematics of plant growth. *Sci Am* 242:134–151.
13. Moreno-Risueno MA, et al. (2010) Oscillating gene expression determines competence for periodic Arabidopsis root branching. *Science* 329:1306–1311.
14. Cosgrove DJ (2005) Growth of the plant cell wall. *Nat Rev Mol Cell Biol* 6:850–861.
15. Ober ES, Sharp RE (2007) Regulation of root growth responses to water deficit. *Advances in Molecular Breeding Towards Salinity and Drought Tolerance*, eds Jenks MA, Hasegawa PM, Jain SM (Springer, New York), pp 33–53.
16. Kramer PJ, Boyer JS (1995) *Water Relations of Plants and Soils* (Academic, San Diego).
17. Verslues PE, Agarwal M, Katiyar-Agarwal S, Zhu J, Zhu J-K (2006) Methods and concepts in quantifying resistance to drought, salt and freezing, abiotic stresses that affect plant water status. *Plant J* 45:523–539.

18. Molz FJ, Boyer JS (1978) Growth-induced water potentials in plant cells and tissues. *Plant Physiol* 62:423–429.
19. Nonami H, Boyer JS (1993) Direct demonstration of a growth-induced water potential gradient. *Plant Physiol* 102:13–19.
20. Silk WK, Wagner KK (1980) Growth-sustaining water potential distributions in the primary corn root: A noncompartmented continuum model. *Plant Physiol* 66:859–863.
21. Wiegers BS, Cheer AY, Silk WK (2009) Modeling the hydraulics of root growth in three dimensions with phloem water sources. *Plant Physiol* 150:2092–2103.
22. Boyer JS, Silk WK, Watt M (2010) Path of water for root growth. *Funct Plant Biol* 37: 1105–1116.
23. Hukin D, Doering-Saad C, Thomas CR, Pritchard J (2002) Sensitivity of cell hydraulic conductivity to mercury is coincident with symplasmic isolation and expression of plasmalemma aquaporin genes in growing maize roots. *Planta* 215:1047–1056.
24. Steudle E, Oren R, Schulze E-D (1987) Water transport in maize roots: Measurement of hydraulic conductivity, solute permeability, and of reflection coefficients of excised roots using the root pressure probe. *Plant Physiol* 84:1220–1232.
25. Ehlert C, Maurel C, Tardieu F, Simonneau T (2009) Aquaporin-mediated reduction in maize root hydraulic conductivity impacts cell turgor and leaf elongation even without changing transpiration. *Plant Physiol* 150:1093–1104.
26. Frensch J, Hsiao TC (1995) Rapid response of the yield threshold and turgor regulation during adjustment of root growth to water stress in Zea mays. *Plant Physiol* 108: 303–312.
27. Melkonian J, Yu LX, Setter TL (2004) Chilling responses of maize (Zea mays L.) seedlings: Root hydraulic conductance, abscisic acid, and stomatal conductance. *J Exp Bot* 55:1751–1760.
28. Nobel PS (2005) *Physicochemical and Environmental Plant Physiology* (Elsevier, Burlington, MA).
29. Steudle E, Boyer JS (1985) Hydraulic resistance to radial water flow in growing hypocotyl of soybean measured by a new pressure-perfusion technique. *Planta* 164: 189–200.
30. Colombo R, Bonetti A, Cerana R, Lado P (1981) Effect of plasmalemma ATPase inhibitors, diethylstilbestrol and orthovanadate, on fusicoccin-induced H^+ extrusion in maize roots. *Plant Sci Lett* 21:305–315.
31. Mesenko MM, Ivanov VB (2005) The effects of H^+-ATPase activator and inhibitors on cell growth in the maize root. *Russ J Plant Physiol* 52:497–503.
32. Morsomme P, Boutry M (2000) The plant plasma membrane H(+)-ATPase: Structure, function and regulation. *Biochim Biophys Acta* 1465:1–16.
33. McMullen MD, et al. (2009) Genetic properties of the maize nested association mapping population. *Science* 325:737–740.
34. Líška D, Martinka M, Kohanová J, Lux A (2016) Asymmetrical development of root endodermis and exodermis in reaction to abiotic stresses. *Ann Bot* 118:667–674.
35. Taramino G, et al. (2007) The maize (*Zea mays L.*) *RTCS* gene encodes a LOB domain protein that is a key regulator of embryonic seminal and post-embryonic shoot-borne root initiation. *Plant J* 50:649–659.
36. Goh T, Joi S, Mimura T, Fukaki H (2012) The establishment of asymmetry in Arabidopsis lateral root founder cells is regulated by LBD16/ASL18 and related LBD/ASL proteins. *Development* 139:883–893.
37. Inukai Y, et al. (2005) *Crown rootless1*, which is essential for crown root formation in rice, is a target of an AUXIN RESPONSE FACTOR in auxin signaling. *Plant Cell* 17: 1387–1396.
38. Lee HW, Kim NY, Lee DJ, Kim J (2009) LBD18/ASL20 regulates lateral root formation in combination with LBD16/ASL18 downstream of ARF7 and ARF19 in Arabidopsis. *Plant Physiol* 151:1377–1389.
39. Okushima Y, Fukaki H, Onoda M, Theologis A, Tasaka M (2007) ARF7 and ARF19 regulate lateral root formation via direct activation of LBD/ASL genes in Arabidopsis. *Plant Cell* 19:118–130.
40. Cutler SR, Rodriguez PL, Finkelstein RR, Abrams SR (2010) Abscisic acid: Emergence of a core signaling network. *Annu Rev Plant Biol* 61:651–679.
41. Steudle E, Peterson CA (1998) How does water get through roots? *J Exp Bot* 49: 775–788.
42. Ibata K, Takimoto S, Morisaku T, Miyawaki A, Yasui M (2011) Analysis of aquaporin-mediated diffusional water permeability by coherent anti-stokes Raman scattering microscopy. *Biophys J* 101:2277–2283.
43. Potma E, de Boeij WP, van Haastert PJ, Wiersma DA (2001) Real-time visualization of intracellular hydrodynamics in single living cells. *Proc Natl Acad Sci USA* 98: 1577–1582.
44. Yu Y-C, Sohma Y, Takimoto S, Miyauchi T, Yasui M (2013) Direct visualization and quantitative analysis of water diffusion in complex biological tissues using CARS microscopy. *Sci Rep* 3:2745.
45. Boyer JS (1995) *Measuring the Water Status of Plants and Soils* (Academic, San Diego).
46. Boersma AJ, Zuhorn IS, Poolman B (2015) A sensor for quantification of macromolecular crowding in living cells. *Nat Methods* 12:227–229.
47. Feng W, Lindner H, Robbins NE, 2nd, Dinneny JR (2016) Growing out of stress: The role of cell- and organ-scale growth control in plant water-stress responses. *Plant Cell* 28:1769–1782.
48. Robbins NE, II, Dinneny J (2016) A method to analyze local and systemic effects of environmental stimuli on root development in plants. *Bio Protoc* 6.
49. Schindelin J, et al. (2012) Fiji: An open-source platform for biological-image analysis. *Nat Methods* 9:676–682.
50. Lowe DG (2004) Distinctive image features from scale-invariant keypoints. *Int J Comput Vis* 60:91–110.
51. R Core Team (2016) R: A Language and Environment for Statistical Computing. Version 3.3.2. Available at https://www.R-project.org/. Accessed January 23, 2017.
52. Wickham H (2011) The split-apply-combine strategy for data analysis. *J Stat Softw* 40: 1–29.
53. Hothorn T, Bretz F, Westfall P (2008) Simultaneous inference in general parametric models. *Biom J* 50:346–363.
54. Pinheiro J, Bates D, DebRoy S, Sarkar D; R Core Team (2016) nlme: Linear and Nonlinear Mixed Effects Models. Version 3.1-128. Available at CRAN.R-project.org/package=nlme. Accessed January 23, 2017.
55. Wickham H (2016) tidyr: Easily Tidy Data with "spread()" and "gather()" Functions. Version 0.6.0. Available at https://CRAN.R-project.org/package=tidyr. Accessed January 23, 2017.
56. Ishida T, Anno T, Matsukawa S, Nagano T (2000) Hydraulic conductivity and diffusion coefficient in gels for plant tissue culture. *Environ Control Biol* 38:165–171.
57. Nobel PS, Cui M (1992) Prediction and measurement of gap water vapor conductance for roots located concentrically and eccentrically in air gaps. *Plant Soil* 145:157–166.
58. Rigby RA, Stasinopoulos DM (2005) Generalized additive models for location, scale and shape. *J R Stat Soc Ser C Appl Stat* 54:507–554.
59. Chang W, Cheng J, Allaire J, Xie Y, McPherson J (2016) Shiny: Web Application Framework for R. Version 0.14.2. Available at https://CRAN.R-project.org/package=shiny. Accessed January 23, 2017.
60. Wickham H (2009) *ggplot2: Elegant Graphics for Data Analysis* (Springer, New York).
61. Wickham H (2016) scales: Scale Functions for Visualization. Version 0.4.1. Available at https://CRAN.R-project.org/package=scales. Accessed January 23, 2017.
62. Urbanek S, Horner J (2015) Cairo: R Graphics Device Using Cairo Graphics Library for Creating High-Quality Bitmap (PNG, JPEG, TIFF), Vector (PDF, SVG, PostScript) and Display (X11 and Win32) Output. Version 1.5-9. Available at https://CRAN.R-project.org/package=Cairo. Accessed January 23, 2017.
63. Kahle D, Wickham H (2013) ggmap: Spatial visualization with ggplot2. *R J* 5:144–161.
64. Bivand R, Lewin-Koh N (2016) maptools: Tools for Reading and Handling Spatial Objects. Version 0.8-39. Available at https://CRAN.R-project.org/package=maptools. Accessed January 23, 2017.
65. Bivand R, Rundel C (2016) rgeos: Interface to Geometry Engine - Open Source (GEOS). Version 0.3-21. Available at https://CRAN.R-project.org/package=rgeos. Accessed January 23, 2017.
66. Andrews S (2010) FastQC: A Quality Control Tool for High Throughput Sequence Data. Version 0.10.1. Available at www.bioinformatics.babraham.ac.uk/projects/fastqc. Accessed January 23, 2017.
67. Buffalo V (2014) Scythe–A Bayesian Adapter Trimmer. Version 0.981. Available at https://github.com/vsbuffalo/scythe. Accessed January 23, 2017.
68. Martin M (2011) Cutadapt removes adapter sequences from high-throughput sequencing reads. *EMBnet J* 17:10–12.
69. Joshi NA, Fass JN (2011) Sickle: A Sliding-Window, Adaptive, Quality-Based Trimming Tool for FastQ Files. Version 1.0. Available at https://github.com/najoshi/sickle. Accessed January 23, 2017.
70. Kersey PJ, et al. (2016) Ensembl Genomes 2016: More genomes, more complexity. *Nucleic Acids Res* 44:D574–D580.
71. Kim D, et al. (2013) TopHat2: Accurate alignment of transcriptomes in the presence of insertions, deletions and gene fusions. *Genome Biol* 14:R36.
72. Trapnell C, et al. (2010) Transcript assembly and quantification by RNA-Seq reveals unannotated transcripts and isoform switching during cell differentiation. *Nat Biotechnol* 28:511–515.
73. Roberts A, Trapnell C, Donaghey J, Rinn JL, Pachter L (2011) Improving RNA-seq expression estimates by correcting for fragment bias. *Genome Biol* 12:R22.
74. Li H, et al.; 1000 Genome Project Data Processing Subgroup (2009) The sequence alignment/map format and SAMtools. *Bioinformatics* 25:2078–2079.
75. Anders S, Pyl PT, Huber W (2015) HTSeq–A Python framework to work with high-throughput sequencing data. *Bioinformatics* 31:166–169.
76. Trapnell C, et al. (2013) Differential analysis of gene regulation at transcript resolution with RNA-seq. *Nat Biotechnol* 31:46–53.
77. Love MI, Huber W, Anders S (2014) Moderated estimation of fold change and dispersion for RNA-seq data with DESeq2. *Genome Biol* 15:550.
78. Reimand J, et al. (2016) g:Profiler–A web server for functional interpretation of gene lists (2016 update). *Nucleic Acids Res* 44:W83–W89.
79. Lawrence CJ, Seigfried TE, Brendel V (2005) The maize genetics and genomics database. The community resource for access to diverse maize data. *Plant Physiol* 138: 55–58.
80. Du Z, Zhou X, Ling Y, Zhang Z, Su Z (2010) agriGO: A GO analysis toolkit for the agricultural community. *Nucleic Acids Res* 38:W64–W70.
81. Saeed AI, et al. (2003) TM4: A free, open-source system for microarray data management and analysis. *Biotechniques* 34:374–378.
82. Ramakers C, Ruijter JM, Deprez RH, Moorman AFM (2003) Assumption-free analysis of quantitative real-time polymerase chain reaction (PCR) data. *Neurosci Lett* 339:62–66.